

Evaluation of polymeric 3D printed adhesively bonded joints: effect of joint morphology and mechanical interlocking

Andrea Spaggiari and Filippo Favali

DISMI, University of Modena and Reggio Emilia, Reggio Emilia, Italy

Abstract

Purpose – The purpose of this paper is to evaluate and exploit the combination of additive manufacturing polymeric technology and structural adhesives. The main advantage is to expand the maximum dimension of the 3D printed parts, which is typically limited, by joining the parts with structural adhesive, without losing strength and stiffness and keeping the major asset of polymeric 3D printing: freedom of shape of the system and low cost of parts.

Design/methodology/approach – The materials used in the paper are the following. The adhesive considered is a commercial inexpensive acrylic, quite similar to superglue, applicable with almost no surface preparation and fast curing, as time constraint is one of the key problems that affects industrial adhesive applications. The 3D printed parts were in acrylonitrile butadiene styrene (ABS), obtained with a Fortus 250mc FDM machine, from Stratasys. The work first compares flat overlap joint with joints designed to permit mechanical interlocking of the adherends and then to a monolithic component with the same geometry. Single lap, joggle lap and double lap joints are the configurations experimentally characterized following a design of experiment approach.

Findings – The results show a failure in the substrate, due to the low strength of the polymeric adherends for the first batch of typical bonded configurations, single lap, joggle lap and double lap. The central bonded area, with an increased global thickness, never does fail, and the adhesive is able to transfer the load both with and without mechanical interlocking. An additional set of scarf joints was also tested to promote adhesive failure as well as to retrieve the adhesive strength in this application. The results shows that bonding of polymeric AM parts is able to express its full potential compared with a monolithic solution even though the joint fails prematurely in the adherend due to the bending stresses and the notches present in the lap joints.

Research limitations/implications – Because of the 3D printed polymeric material adopted, the results may be generalized only when the elastic properties of the adherends and of the adhesive are similar, so it is not possible to extend the findings of the work to metallic additive manufactured components.

Practical implications – The paper shows that the adhesives are feasible way to expand the potentiality of 3D printed equipment to obtain larger parts with equivalent mechanical properties. The paper also shows that the scarf joint, which fails in the adhesive first, can be used to extract information about the adhesive strength, useful for the designers which have to combine adhesive and additive manufactured polymeric parts.

Originality/value – To the best of the researchers' knowledge, there are scarce quantitative information in technical literature about the performance of additive manufactured parts in combination with structural adhesives and this work provides an insight on this interesting subject. This manuscript provides a feasible way of using rapid prototyping techniques in combination with adhesive bonding to fully exploit the additive manufacturing capability and to create large and cost-effective 3D printed parts.

Keywords Adhesives, 3D printing, Polymeric additive manufacturing, Bonded joints, Design of experiments

Paper type Research paper

1. Introduction

The increasing use of lightweight materials such as carbon or glass fibre-reinforced composites has fostered the adhesive bonding technology as a reliable method to join different parts in a mechanical assembly, where stiffness and weight are crucial constraints, such as in aerospace and automotive industries (Banea *et al.*, 2018; Koricho *et al.*, 2016; Scarselli *et al.*, 2017; Vijaya Kumar *et al.*, 2013). Several advantages can be obtained with adhesives when compared to traditional mechanical

joining techniques such as welding, riveting or threaded connections. Firstly, the adhesives do not require any holes in the substrate, which is detrimental to the structural integrity of the fibres; secondly, the adhesives allow the designer to join different materials with a smooth load distribution along the entire bondline, and finally, the adhesives are applicable with an increasing degree of automation, which is fundamental to

The current issue and full text archive of this journal is available on Emerald Insight at: <https://www.emerald.com/insight/1355-2546.htm>



Rapid Prototyping Journal
28/8 (2022) 1437–1451
Emerald Publishing Limited [ISSN 1355-2546]
[DOI 10.1108/RPJ-09-2021-0259]

© Andrea Spaggiari and Filippo Favali. Published by Emerald Publishing Limited. This article is published under the Creative Commons Attribution (CC BY 4.0) licence. Anyone may reproduce, distribute, translate and create derivative works of this article (for both commercial and non-commercial purposes), subject to full attribution to the original publication and authors. The full terms of this licence maybe seen at <http://creativecommons.org/licenses/by/4.0/legalcode>

Received 30 September 2021
Revised 20 December 2021
2 February 2022
Accepted 7 February 2022

lower the manufacturing costs (Adams, 2021). On the other hand, several drawbacks are typical of this technique, such as the technological need for surface preparation (Alfano *et al.*, 2012; Broad *et al.*, 1999; Critchlow *et al.*, 2006), which is not easy to handle in an industrial environment, and the presence of an elastic mismatch between adhesive and adherends, which causes stress peaks at the bondline corners and promotes premature failure of the joint. Except for special test coupons such as the napkin ring (Adams *et al.*, 1997), the Iosipescu specimen (IOSIPESCU and N., 1967; Stojcevski *et al.*, 2018) and a four point bending test (Spaggiari *et al.*, 2016; Wycherley *et al.*, 1990), which allow the shear stresses to be present with no or moderate stress concentrations, the strong difference in the elastic properties of the materials causes severe stress concentrations, especially in the peel direction, when the adhesive properties are retrieved from the thin layer (Carpenter, 1989; Crocombe *et al.*, 1990; Goland and Reissner, 1944). The scientific literature reports some methods to lower the degree of singularity of these peaks, such as a slight modification of the adherends (F M da Silva and D Adams, 2007; Liao *et al.*, 2013) or spew fillet (Gay *et al.*, 2002; Tsai and Morton, 1995) and relief grooves (Castagnetti, Spaggiari, *et al.*, 2010; Choupani, 2008; da Silva *et al.*, 2010; Spaggiari *et al.*, 2012, 2013). By using modern techniques and introducing additive manufacturing considerations, some researchers considered the possibility of lowering stress concentrations by reducing the adherends stiffness, or by increasing the adhesive stiffness with functionally graded materials (Apalak, 2006; Zhang *et al.*, 2012), but at the moment, these approaches are limited to speculative concepts and niche applications, as the technology is not yet at a readiness level suitable to implement these findings. Nevertheless, additive manufacturing (AM) has become a widespread technology and could play an important role in the solution of some of these problems. While selective laser sintering (SLS), selective laser melting (SLM) or electron beam (EB), are quite common for AM of metal parts, the most typical and widespread method for polymers is fused deposition molding (FDM), which is quite inexpensive, reasonably fast and produces ready-made 3D printed parts with a decent surface finish.

AM components could be designed with extreme shape liberty, thus this technique is ideal improve the performances of adhesive bonded joint in terms of strength compared to the traditional solutions, as the stiffness of the metal AM part can be artificially lowered without affecting the external geometry by using metamaterial concepts such as lattice structures or hollow components (Dragoni, 2013; Ubaid *et al.*, 2018). This may lead to a similar level of stiffness between the adhesive and the adherends and also adds a positive effect in terms of lightweight design. In addition, by combining AM and adhesive bonding it is easy to overcome one of the actual limitations of the AM technology, which is the small working volume of the AM machines (at least for the entry level ones). Many 3D printers can easily produce small components (a typical reference volume is $250 \times 250 \times 250$ mm), but the scalability to larger dimensions is not a trivial task. As soon as the volume increase, material distortions arise, stability of thin-walled structures (i.e. where the thickness is below 1/10 of the main linear dimensions) drops, and therefore, the tolerances and the cost of investment are non-linearly

dependent on the maximum dimension of the printed component. Therefore, as reported in recent technical literature (Spaggiari and Denti, 2019), combining the adhesive bonding and the AM manufacturing presents several advantages: Firstly, it exploits fully the AM device capability; secondly, it increases the dimensional range of AM applications and third, it brings the mechanical resistance of the adhesively bonded AM joint to the same level of the base polymeric material. To date, the mechanical characterization of the AM components or adhesive joints can be traced in the literature, but the interactions of AM parts bonded with structural adhesives has not been deeply investigated yet, with only partial studies about the bonding of AM plastic components being available (Garcia and Prabhakar, 2017; Kariz *et al.*, 2017). The possibility to add mechanical interlocking is an additional feature, which improves the adhesion, with the typical substrates used in AM, either metallic or polymeric, as studied in Dugbenoo *et al.* (2018) for composite parts. This work aims at the design, manufacturing, and experimental verification of the mechanical properties, mainly strength and stiffness, of bonded AM parts with and without mechanical interlocking by providing a comparison with traditional bonding on flat surfaces or with monolithic joints printed directly as unique parts.

The manuscript aims at evaluating the performance of the bonded parts compared to the monolithic ones and to quantify the effect of the mechanical interlocking, if any. The manuscript contributes to provide information about the applicability of adhesives to expand the 3D printed parts to larger dimensions without losing mechanical strength or stiffness. The study reveals how the 3D printed parts could be joined with adhesives considering the failure mode as well (inside the adhesive or in the 3D printed substrate). A possible criterion taken from literature based on structural stresses is used to provide a simple insight of the joint strength and consider also the presence of shear and peel stresses at the bondline edges.

2. Materials and method

2.1 Design plan

The first set of tests is performed following the methodology already carried out in Spaggiari and Denti (2019) and is focused on the test of the bonded AM polymeric material by means of several lap joints configurations. A Design of Experiment (DoE) approach was adopted, where the variables are the configuration geometry and the connection morphologies. A first set of tests on standard lap joints (not reported here for the sake of brevity) was used to assess the mechanical behaviour and to come up with an optimized geometry. The parts were produced using a Stratasys Fortus 250 mc printer (Stratasys, 2018), which grants a reliable repeatability of the specimens and a quasi-full dense filling of the ABS specimens. The specimen dimensions were decided after the first set of preliminary tests, as ASTM standards are hardly applicable to AM technology. The printing parameters are recalled in Table 1.

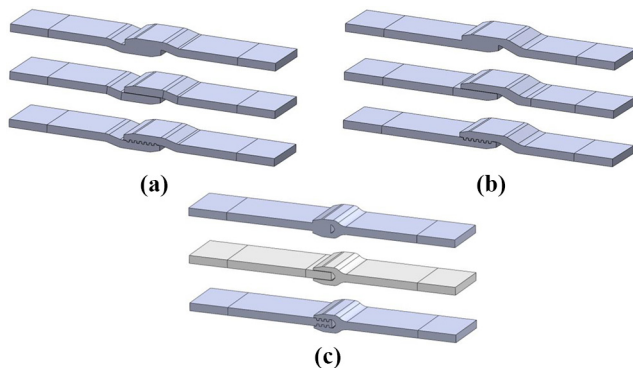
The first test campaign was set up on three different geometries: a symmetric single lap (SSL) joints, which ensures

Table 1 Printing parameters used to print the specimen with the Stratasys Fortus 250 mc

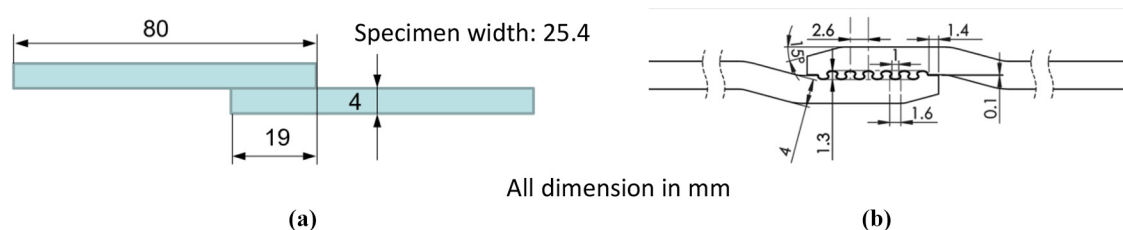
3D printing parameter	
Filament size	1.78 mm
Melting temperature	298°C
Environment temperature	75°C
Layer thickness	0.1778 mm
Infill geometry	Solid: no raster
Infill density	Above 98%
Printing speed	1 cm ³ /h on average
Printing direction	Always on joint side

good alignment of the bonded area with the force direction, an asymmetric joggle lap (AJL) joint, which presents a geometrical difference between the two adherends, a double lap (DL) joint which was designed to have the same nominal bonded area of the first two, to provide a fair comparison. In addition to the flat bonded joints, a monolithic configuration was added as reference, obtained by printing directly with AM the whole joint and also an interlocking configuration was designed and tested. The idea is to exploit the extreme freedom of shape granted by the AM technology to improve the joining performance by adding a series of “teeth” in the bonding area. These teeth introduce many possible benefits to the joint:

- 1 an increase of the bonding area;
- 2 add the interlocking effect decreasing the opening of joints due to peel stresses; and

Figure 1 Lap joint tested SSL joint (a), AJL joint (b), and DL joint (c)

Notes: All the geometries are tested in monolithic, flat and interlocking configurations, as shown from top to bottom

Figure 2 Main dimensions of the lap joint (a) and detail of the interlocking tooth common to all geometries (b)

All dimension in mm

- 3 an increase the precision of coupling during the bonding operations.

As a drawback one can foresee a larger stress concentration factor, which could be detrimental for the performances especially on polymeric materials. The trade-off between pros and cons is quantitatively explored by carrying out a series of experimental tests. The CAD models of the joints and the configurations are reported in [Figure 1](#), while the global dimension dimensions of the joints are reported in [Figure 2\(a\)](#). The tooth geometry was optimized with respect to the shape, the number of teeth and height, after some preliminary tests. It was decided to use a fixed number of teeth on the bondline (six) and a round profile, which is easier to obtain with the AM. The peak to valley depth of the tooth is 1.20 mm to avoid a deep cut in the section of the joint and, therefore, a strong decrease in the net area. A detail of the tooth with the main dimensions is reported in [Figure 2\(b\)](#).

The last configuration printed was a monolithic component obtained by merging the two joints directly in the CAD model and printing the whole assembly together, which gives the authors a reference value to which the bonded ones could be compared. These joints were bonded with Henkel Loctite 401, a single component cyanoacrylate adhesive. The adhesive behaviour when applied to 3D printed polymeric parts is comparable to Hysol 4070, a double component epoxy resin produced for AM parts, already considered in by [Spaggiari and Denti \(2019\)](#), but the 401 is less expensive, simpler to use and faster to cure. The technical properties of Loctite 401 are reported by the manufacturer in the TDS ([Loctite, 2012](#)).

The experimental variables were arranged according a DoE ([Montgomery, 2004](#)) multilevel factorial design plan ([Mead et al., 2012](#)). This methodology has several advantages, in particular, it provides an easy statistical interpretation of the results and an increased reliability of the findings. The levels and variables considered are summarized in [Table 2](#), while the system responses considered are: the maximum non-dimensional load and the joint stiffness. Five specimens were printed for each bonded configuration (replicates) for a total of 30 bonded joints. The number of replicates were reduced to three for the monolithic joints (a total of nine joints) as a lower variability without the adhesive was expected. The maximum loading force and the effective stress were recorded. The non-dimensional load was defined as the ratio between the experimental measured peak force and the base material force given by the same net area, which is defined later on in the Experimental test section. This parameter provides a straightforward comparison of the joint regardless of the

Table 2 Experimental plan of the first set of joints

Joint geometry	Symmetric single lap	Joggle lap	Double lap
Surface profile	Flat	Mechanical interlocking	Monolithic
Replicates	5 for bonded configuration, 3 for monolithic configuration		
System response	Maximum non-dimensional load		Joint stiffness

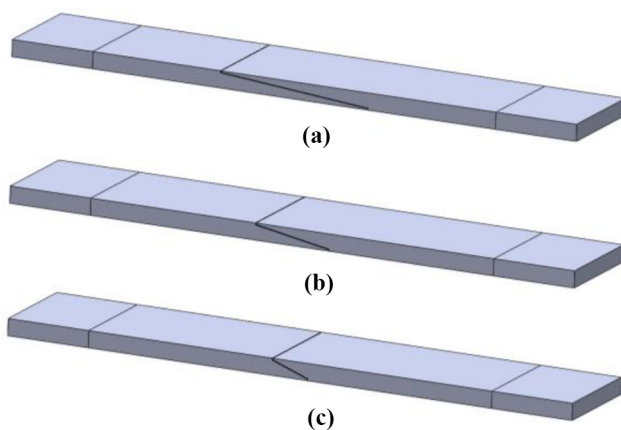
material used to print them. A summary of this first batch of joints is presented in Table 1.

An additional configuration of flat scarf joint was tested after the first set of samples since the majority of the ruptures occurred in the base material and not in the adhesive, as shown in the results and discussion section. The scarf joint was selected, as it presents the unique feature of being able to perfectly mimic the monolithic material due to its continuous and uniform thickness throughout the joint, including the joining region, and avoids any overlap part of the joint with double global thickness similarly to the SSL and ASJ joints, or even triple global thickness as in the case of DL joints. The scarf joint (SJ) is thinner than the DL, AJL and SSL so in this case it was not possible to design a mechanical interlocking profile. Therefore, only the flat condition was tested, considering three different scarf angles (5° , 10° , 20°) to evaluate the influence of the angle on the joint performance, as shown in Figure 3. The mean configuration with the angle of 10° was defined to have the same bonding area as in the flat DL, AJL and SSL, which leads to a nearly double area with a 5° angle scarf joint to a nearly half bonding area with 20° angle.

2.2 Experimental set up

The specimens were printed with a Stratasys - Fortus 250mc and bonded with the Loctite 401 following the standard recommendations to grant proper polymerization and alignment. All the specimens were printed oriented on the side at full density, to achieve good mechanical properties of the ABS substrate up to 33 MPa according to the producer (Stratasys, 2019). A set of dog-bone specimen

Figure 3 Flat scarf joints tested, from 5° angle (a), 10° angle (b) and 20° angle (c)



Notes: Note that the thickness of 4 mm is constant throughout the entire joint length

was printed together with the adherends and tested to verify this value (reported in Figure A2 of the Appendix) with an ultimate tensile stress of 35.46 MPa, values which are slightly higher than the datasheet indications. This latter value is used to compare the performance of the scarf joint. A specific test rig was used to enforce the relative position of the parts, and the Loctite 7030 Cleaner was used to remove possible superficial debris on the bonding area. No mechanical or chemical surface treatments were applied, even though these procedures increase the adhesive strength (Chen *et al.*, 1997; Packham, 2003), as the surface was already tailored with the 3D printer. One of the aims of the present work is in fact to show whether 3D printed parts can be effectively and efficiently bonded with ease skipping the complex, expensive and time-consuming procedures typical of metallic prints. The first batch of bonded specimens is reported in Figure 4, divided by types. All the selected specimens were bonded with a nominal adhesive thickness of 0.1 mm, which was guaranteed by the geometry of the joint itself. A simple experimental rig was used to ensure the alignment between the joints and the adhesive thickness as well, so that the position of the bonded parts is automatically enforced by gravity and mechanical stops. More information on the test rig is added in Figure A1 in the Appendix section.

All the joints were cured at room temperature and relative humidity of 50% for 24 h, which largely exceed the prescribed polymerization time of 5 min on ABS (Loctite, 2012). The detail of the joints, both for flat and interlocking condition is reported in Figure 5. The experimental set up is shown in Figure 6: a quasi-static displacement to the specimens was applied by means of a universal tensile machine (Galdabini SUN 500), equipped with a 5000 N load cell. The applied crosshead displacement is 1 mm/min, to avoid possible viscoelastic effects, both for the adherends and the adhesive. The joint geometries were chosen to be symmetrical with respect to the force applied and therefore the correct alignment of the specimens with the machine grippers is automatically enforced and no alignment tabs are needed.

Figure 4 3D printed specimens before bonding with Loctite 401



Figure 5 The SSL joints (a), AJL joints (b) DL joints (c) both for flat (upper) and interlocking (lower) geometries; detail of the bonding for the scarf joint with 5°, 10° and 20° angle from top to bottom (d)

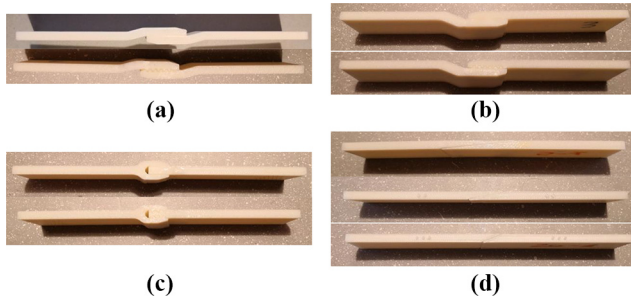


Figure 6 Experimental tensile test on double lap bonded joints



2.3 Finite element analysis of the scarf joints

To better understand the scarf joint behaviour, a finite element analysis of the scarf joints was carried out. The joints were subjected to experimental force measured during the tests

(reported in [Figure 9](#)) to evaluate the stress distribution in the adhesive layer, using the Solidworks Simulation software. A linear elastic material was used as well as the mechanical properties obtained by the datasheets of the adhesive and the ABS. The adhesive thickness is constant (0.1) mm due to the surface roughness of the ABS. The model is planar, with plane strain elements both for adhesive and adherends. The mesh is refined in the adhesive region with an average dimension of 0.03 mm, while in the adherends the average dimension is 0.5 mm, with a gradual transition between the two values given by the automatic mesh routine. The contact constraint used to enforce the bonding is a surface-to-surface constraint, which bonds every node of the adherends to the corresponding node on the adhesive. The model loading scheme is reported in [Figure 7\(a\)](#), a detail of the mesh refinement is provided in [Figure 7\(b\)](#), where it is also highlighted the midline where the stresses will be retrieved. The contact constraint used to enforce the bonding is a surface-to-surface constraint, which bonds every node of the adherends to the corresponding node on the adhesive.

3. Results

3.1 Experimental results

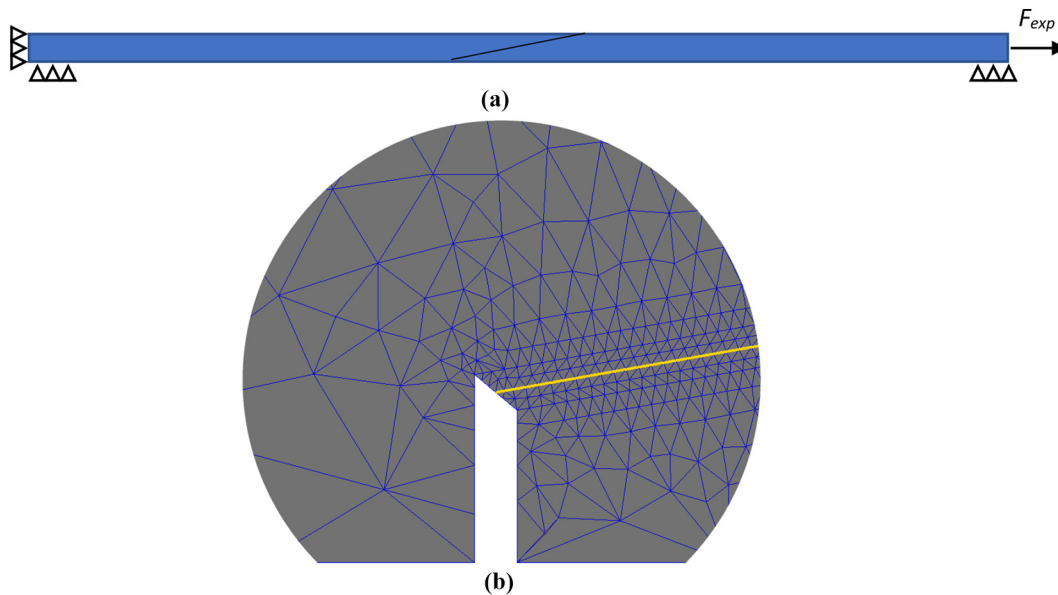
The comparison of several geometries tested is carried out based on the force displacement curves recorded following the procedure described in Section 2.2. [Figure 8](#) shows the curves for the three configurations (DL, AJL, SSL) for flat, monolithic, interlocking joints. [Figure 9](#) shows the curves for the three angled flat scarf joints. [Figure 10](#) shows the two typical failure modes found for the joints. The lap joints with the adhesive entrapped in a sandwich of substrate material with a global thickness nearly double (SSL, AJL) or triple (DL) of the adherend fail in the substrate. On the other hand, the scarf joint with constant thickness fails in a mixed mode: first the crack proceeds in the adhesive, then the adherend fails, as it was clearly visible and audible during the experimental tests. As the scarf joints present an adhesive failure, at least initially, these joints are the only ones which could be used to provide information on the adhesive strength. Therefore, a deeper analysis was carried out on these joints to provide a better understanding of the adhesive behaviour, when applied to AM parts.

4. Discussion

4.1 Main experimental plan

All the joints tested in the main experimental plan failed in the substrate, so in this case no conclusion can be drawn on the adhesive properties other than the fact that the adhesive is strong enough to completely transferring the load to the adherends. This corroborates the hypothesis that bonding 3D printed polymeric parts does not cause a lower strength or stiffness of the structure. Anyhow some differences arise between the bonded joints (flat or with interlocking) and the monolithic ones. Two mechanical responses were extracted by the analysis of the experimental results: the maximum relative load [[Figure 11\(a\)](#)] and the stiffness of the joint [[Figure 11\(b\)](#)]. The maximum relative load is obtained by dividing the experimental maximum force (as reported in [Appendix Table A1](#)) by the average force obtained using the standard test on dog-bone

Figure 7 FE model loading scheme, scale 1:1 (a), mesh details with the midline of the adhesive in yellow (b)



specimens of the base material (3545 N). Figure 11(a) shows some interesting trends. Firstly, it can be noted that the results are divided by joint type, monolithic, flat and interlocking. The scarf joints are reported in the flat configuration only as it was not possible to manufacture them in the interlocking configuration due to their thin profile. Obviously, the monolithic configuration is simply a base material specimen, and it is not relevant. Among the three configuration it is evident that the monolithic ones are not the strongest in term of relative force, which is quite surprising. The best performance is obtained by flat specimen both for double lap joints and symmetric single lap. Only the asymmetric joggle lap, which in any case shows the lowest performance overall, has a slightly better behaviour in monolithic configuration. The interlocking surface confirms the findings of Spaggiari and Denti (2019), as it does not provide any benefits to the joints in terms of maximum strength. An analysis of variance of the peak force and stiffness was performed and the results, reported in the Appendix (Figure A3) confirm that both the maximum force and the stiffness depends strongly on the joints configuration and to a lesser extent on the surface profile. The interaction of the variables is slightly significant as well. This behaviour could be explained by considering the fact the adhesive mechanics in bonded joints is typically ruled by the differential deformation between the upper and lower adherend, which cause a strong strain of the adhesive (Bigwood and Crocombe, 1989; Carpenter, 1989; Goland and Reissner, 1944), which concentrates at the edges, both for peel and shear stresses. In case of polymeric AM joints the elastic modulus of the substrate (2200 MPa from the TDS) is comparable with the adhesive modulus of the adhesive. The latter is not provided by the producer and scarce information are retrievable, but for a typical cyanoacrylate is between 1200 and 1400 MPa (Matweb, 2021), so adhesive and the adherend have roughly the same stiffness. In terms of mechanical strength, the TDS of the adhesive reports an average stress for the single lap joint made in ABS of 7.5 MPa, which would lead, considering the bonded area of 482.6 mm² for the flat joint [Figure 2(a)] to a force of around 3.6 kN, which comparable to the substrate uniaxial tensile maximum load.

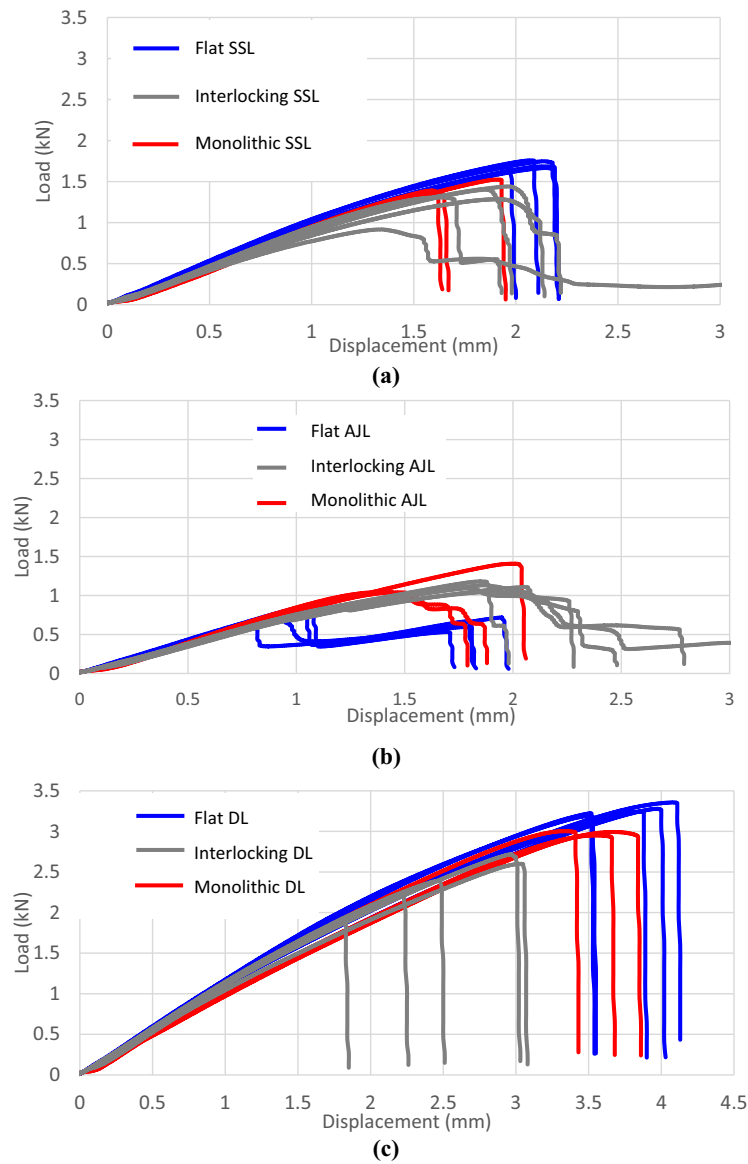
Thus, on one hand, the adhesive is not triggered by the elastic mismatch and on the other hand the load carrying capacity and the strength of the adhesive exceeds the adherends' failure load, which explains the failure of the substrate in almost all the joint tested, as in the example shown in Figure 10(a). It is important to note that this explanation holds only for polymeric adherends, while it would have been completely different with metallic ones, as the adherends' failure load is never reached and the elastic mismatch is typically from 30 to 100 times. The slightly better performance of the bonded joints is to be found in the brittle behaviour of the 3D printed ABS and its sensitivity to notches (Ng *et al.*, n.d.; Roberson *et al.*, 2015; Torrado Perez *et al.*, 2014). It can be seen from a qualitative standpoint that the fracture originates at the end of the bondline, where the stresses are higher, and then propagates faster in a monolithic material, while in case of the bonded joint, the two interfaces between upper and lower adherends and the adhesive provide an additional amount of energy to be dissipated in the joint.

4.2 Scarf joints finite element (FE) discussion and adhesive failure behaviour

In the case of the scarf joint, the fracture mode is quite different, as regardless of the size of the angle, the fracture initially starts in the adhesive and only after the debonding of a large portion of area the adherend fails [Figure 10(b)]. Obviously for lower angles a larger bonded area is involved and therefore the maximum load is higher, but the drop in maximum force is not proportional to the bonded area. In Figure 12(a)-(b), the contour of the peel stress and shear stress are reported respectively, limited at 60 MPa to estimate the full field distribution, as the peak stress at corners, where the singularity arises, is not relevant in this case of linear elastic analysis.

As strong stress concentrations are present at the edges of the bondline (Adams and Wake, 1986), as shown in Figure 12(a)-(b), and the analysis is linear elastic, the structural stresses in the middle of bondline [Figure 7(b)] were

Figure 8 Experimental load displacement curves for SSLs (a) AJLs (b) and DLJs (c) Notes: Blue curves represent the flat configuration, grey curves the interlocking joints and red curves the monolithic ones



Notes: Blue curves represent the flat configuration, grey curves the interlocking joints and red curves the monolithic ones

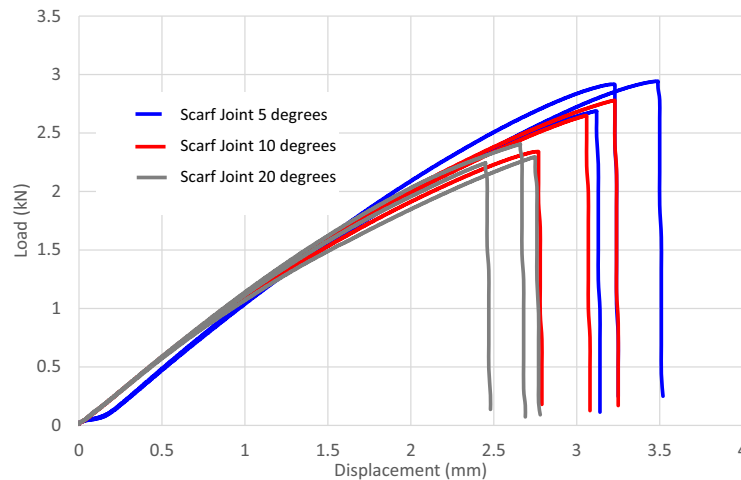
considered as proposed in (Bigwood and Crocombe, 1989; Castagnetti *et al.*, 2009; Castagnetti, Dragoni, *et al.*, 2010; Dragoni *et al.*, 2010; Goglio *et al.*, 2008) to avoid the peak stress at the edges. Figure 13 reports the structural stresses along the normalized bondline for the three scarf joint configurations considered, blue squares for the 5°, orange crosses for the 10° and grey dots for the 20° configuration. The normalization of the bondline length is needed as different angles define different bond-lengths. The stresses are extracted in the middle of the bondline by considering a coordinate system aligned with the line of Figure 7(b). The peak structural stress triggers the adhesive failure and, as shown in Table 3, the value of the shear and the peel stresses are comparable regardless of the angle, while the average stress, defined as the

maximum experimental force over area, is not useful for a comparison and must be disregarded.

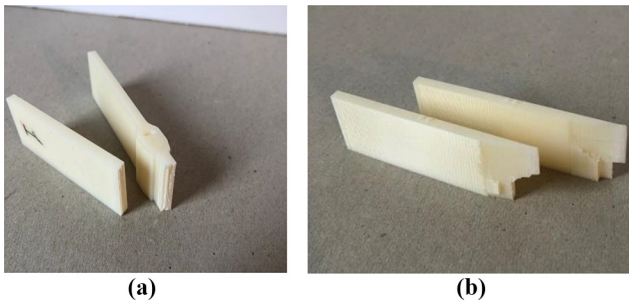
It is also possible to estimate a structural critical stress by considering the criterion proposed by Spaggiari *et al.* (2019), which states that the critical stress is based on the equation (1):

$$\tau_{cr} = \sqrt{\tau^2 + A\sigma} \quad (1)$$

where the parameter A must be retrieved experimentally and σ and τ are given by the FE analyses. According to the scientific literature, this criterion works with stresses which are not affected by stress concentrations (Spaggiari *et al.*, 2019). In this case, severe stress concentrations arise at the edges, but the structural stresses computed in the middle of the bondline are

Figure 9 Experimental load displacement curves for flat scarf joints

Notes: Blue curves represent the 5° configuration, red curves the 10° configuration and the grey ones the 20° configuration

Figure 10 Different failure modes for the specimens considered a substrate failure for the double lap joint (a) and mixed failure (adhesive first than substrate) (b) for the scarf joint

less affected by these singularities; therefore, it seems reasonable to apply the proposed criterion. Considering the values in Table 3, extracted from the charts in Figure 13(a) for normal (peel) stresses and Figure 13(b) for shear stress, it is quite simple to verify that with $A = 30$ MPa, the critical structural stress is on average 58.5 MPa for every angle considered. Having a unique critical structural stress for several angles confirms that the criterion seems applicable to structural stresses as well:

$$\begin{aligned} \text{Critical structural stress Scarf angle } 5^\circ \\ \rightarrow \sqrt{44.42^2 + 30 \cdot 40.12} = 59.5 \text{ MPa} \end{aligned}$$

$$\begin{aligned} \text{Critical structural stress Scarf angle } 10^\circ \\ \rightarrow \sqrt{43.7^2 + 30 \cdot 36.8} = 57.4 \text{ MPa} \end{aligned}$$

$$\begin{aligned} \text{Critical structural stress Scarf angle } 20^\circ \\ \rightarrow \sqrt{47.15^2 + 30 \cdot 33.87} = 58.4 \text{ MPa} \end{aligned}$$

5. Conclusions

Once analysed and discussed all the experimental results previously exposed, it has been possible to reach the following conclusions:

- The present work demonstrated the possibility to exploit the combination of additive manufacturing polymeric technology and structural adhesives. On one hand, it exploits the liberty of form given by the AM, and on the other hand, it increases at no cost the dimensions of the final parts.
- The use of a fast-curing cyanoacrylate, inexpensive and applicable without any surface preparation is possible and provides good bonding, deleting one the problems which often undermines the use of adhesives industrial applications.
- The use adhesive does not compromise the load carrying capacity of the joint for the most common configuration of bonded joints, single lap, joggle lap and double lap analysed, as the joints fail always in the polymeric substrate.
- On the one hand, the substrate failure confirms that the application of adhesive to AM parts is feasible, and on the other hand, it prevents a comparison on the effect of flat or interlocked bonding joints.
- In most cases, the best performance in terms of peak force and joint stiffness is obtained with flat bonded joints, as confirmed by an ANOVA of the results. This finding simplifies the joint design of polymeric AM parts, as no complex feature must be obtained in the bonded area.
- The results in term of load carrying capacity and stiffness of the bonded AM parts are comparable with the base material and better for the bonded joints compared to the monolithic ones.
- The only configuration which experimentally shows the adhesive to fail before the adherends is the scarf joint, as there are no bending stresses in the substrate and the joint regions does not have a double thickness compared to the adherends.

Figure 11 Results of the experimental test in terms of relative maximum force (a) and stiffness (b) for the DL, AJL SSL and scarf joints, with standard deviation bars

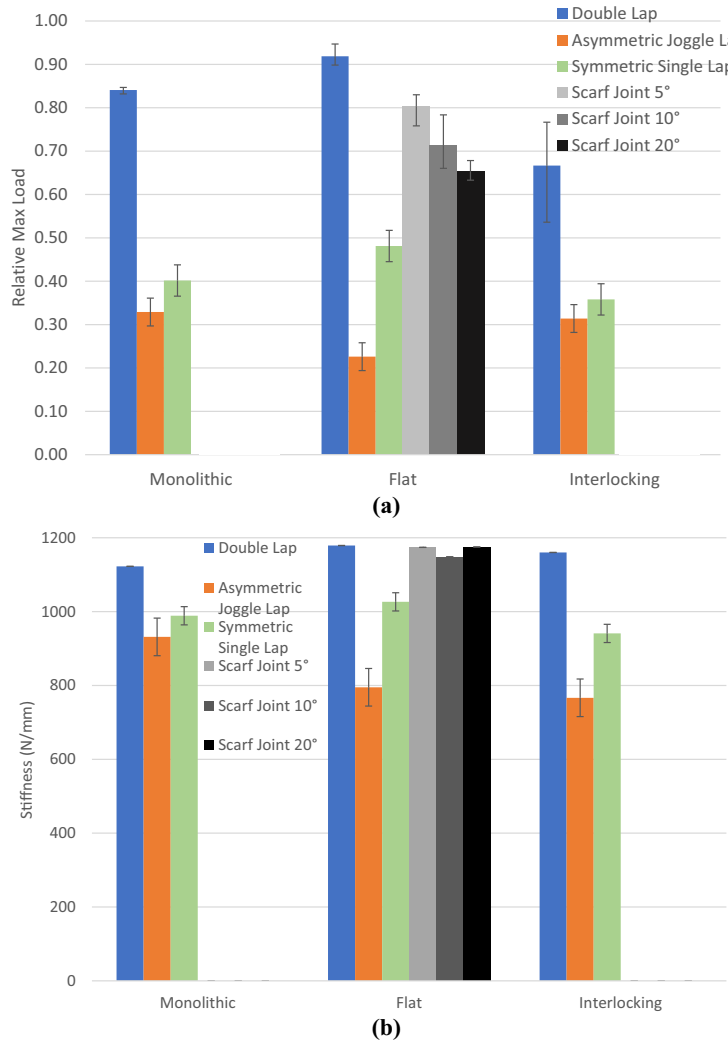


Figure 12 Contours of peel (c) and shear (d) stresses in the bonded region for the 10° scarf joint(c), considering a reference system oriented along the bondline length

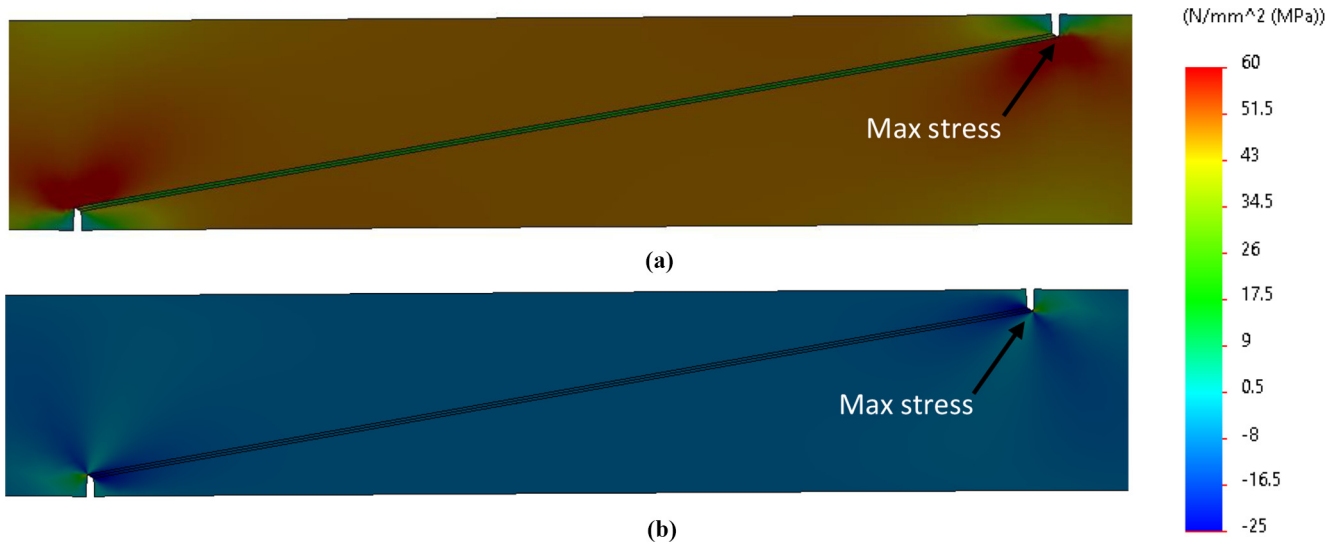


Figure 13 Structural normal (a) and shear (b) stress computed in the middle of the bondline for the three-scarf joint under the experimental average force

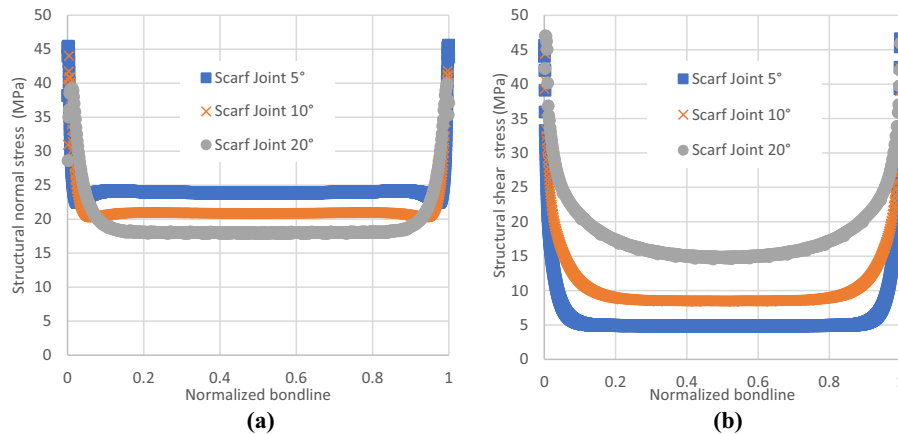


Table 3 Relevant values for scarf bonded joints

Values	Scarf joint 5°	Scarf joint 10°	Scarf joint 20°
Average peak force, applied in FE models (N)	2849	2589	2315
Bonded area (mm ²)	933	468	238
Average stress (MPa)	3.05	5.53	9.74
Structural peak peel stress on the midline (MPa)	45.58	44.01	39.9
Structural peak shear stress on the midline (MPa)	46.58	44.44	47.02
Critical structural stress obtained with equation (1) (MPa)	~ 58.5		

- The results for the scarf joints indicate a good behaviour of this joint as well, which provides a stiffness comparable to the double lap joint and a load carrying capacity of around 80% of the base material for the lowest angle tested (5°).
- A simple stress-based criterion approach found in technical literature seems to be applicable for the adhesive also in this case if combined with structural stresses far enough from the corner singularities.
- This work provides quantitative insight on the mechanical behaviour of the bonded joints, which could lead to an expansion of the capability of AM polymeric technologies to large parts without the need of expensive equipment.

Future works will include an expansion of the application of adhesives to AM parts under more complex loading condition, such as bending or torsion and the evaluation of the joint properties as a function of the test temperature.

References

- Adams, R.D. (2021), *Adhesive Bonding: Science, Technology and Applications*, 2nd ed., Elsevier.
- Adams, R.D. and Wake, W.C. (1986), *Adhesive Joints in Engineering*, doi: [10.1007/978-94-009-5616-2](https://doi.org/10.1007/978-94-009-5616-2).
- Adams, R.D., Comyn, J. and Wake, W.C. (1997), “Structural adhesive joints in engineering”, *Structural Adhesive Joints in Engineering*, Springer, Chapman and Hall.
- Alfano, M., Lubineau, G., Furguele, F. and Paulino, G.H. (2012), “Study on the role of laser surface irradiation on damage and decohesion of Al/epoxy joints”, doi: [10.1016/j.ijadhadh.2012.03.002](https://doi.org/10.1016/j.ijadhadh.2012.03.002).
- Apalak, M.K. (2006), “Elastic stresses in an adhesively-bonded functionally-graded tubular single-lap joint in tension”, *Journal of Adhesion Science and Technology*, Taylor & Francis, Vol. 20 No. 9, pp. 1019-1046.
- Banea, M.D., Rosioara, M., Carbas, R.J.C. and da Silva, L.F.M. (2018), “Multi-material adhesive joints for automotive industry”, *Composites Part B: Engineering*, Elsevier, Vol. 151, pp. 71-77.
- Bigwood, D.A. and Crocombe, A. (1989), “Elastic analysis and engineering design formulae for bonded joints”, *International Journal of Adhesion and Adhesives*, Vol. 9 No. 4, pp. 229-242.
- Broad, R., French, J. and Sauer, J. (1999), “CLP new, effective, ecological surface pretreatment for highly durable adhesively bonded metal joints”, *International Journal of Adhesion and Adhesives*, Vol. 19 Nos 2/3, pp. 193-198.
- Carpenter, W.C. (1989), “Goland and reissner were correct”, *The Journal of Strain Analysis for Engineering Design*, Vol. 24 No. 3, pp. 185-187.
- Castagnetti, D., Dragoni, E. and Spaggiari, A. (2009), “Efficient post-elastic analysis of bonded joints by standard finite element techniques”, *Journal of Adhesion Science and Technology*, Vol. 23 Nos 10/11, pp. 1459-1476.
- Castagnetti, D., Dragoni, E. and Spaggiari, A. (2010), “Failure analysis of bonded T-peel joints: efficient modelling by

- standard finite elements with experimental validation”, *International Journal of Adhesion and Adhesives*, Vol. 30 No. 5, pp. 306-312.
- Castagnetti, D., Spaggiari, A. and Dragoni, E. (2010), “Robust shape optimization of tubular butt joints for characterizing thin adhesive layers under uniform normal and shear stresses”, *Journal of Adhesion Science and Technology*, VSP, an imprint of Brill, Vol. 24 Nos 11/12, pp. 1959-1976.
- Chen, S., Ono, S., Teii, S. and Yoshino, T. (1997), “Improvement of the adhesion of the resin to the metal surface by using plasma jet”, *Surface and Coatings Technology*, Vol. 97 No. 1-3, pp. 378-384.
- Choupani, N. (2008), “Mixed-mode cohesive fracture of adhesive joints: experimental and numerical studies”, *Engineering Fracture Mechanics*, Vol. 75 No. 15, pp. 4363-4382.
- Critchlow, G.W., Yendall, K.A., Bahrani, D., Quinn, A. and Andrews, F. (2006), “Strategies for the replacement of chromic acid treatments for the structural bonding of aluminium alloys”, *International Journal of Adhesion and Adhesives*, Vol. 26 No. 6, pp. 419-453.
- Crocombe, A.D., Bigwood, D.A. and Richardson, G. (1990), “Analysing structural adhesive joints for failure”, *International Journal of Adhesion and Adhesives*, Vol. 10 No. 3, pp. 167-178.
- da Silva, L.F.M., Ferreira, N.M. A J., Richter-Trummer, V. and Marques, E. A S. (2010), “Effect of grooves on the strength of adhesively bonded joints”, *International Journal of Adhesion and Adhesives*, Elsevier, Vol. 30 No. 8, pp. 735-743.
- Dragoni, E. (2013), “Optimal mechanical design of tetrahedral truss cores for sandwich constructions”, *Journal of Sandwich Structures & Materials*, SAGE Publications Sage UK, London, England, Vol. 15 No. 4, pp. 464-484.
- Dragoni, E., Goglio, L. and Kleiner, F. (2010), “Designing bonded joints by means of the JointCalc software”, *International Journal of Adhesion and Adhesives*, Vol. 30 No. 5, pp. 267-280.
- Dugbenoo, E., Arif, M.F., Wardle, B.L. and Kumar, S. (2018), “Enhanced bonding via additive manufacturing-enabled surface tailoring of 3D printed continuous-fiber composites”, *Advanced Engineering Materials*, John Wiley & Sons, Ltd, Vol. 20 No. 12, p. 1800691.
- F M da Silva, L. and D Adams, R. (2007), “Techniques to reduce the peel stresses in adhesive joints with composites”, *International Journal of Adhesion and Adhesives*, Vol. 27 No. 3, pp. 227-235.
- Garcia, R. and Prabhakar, P. (2017), “Bond interface design for single lap joints using polymeric additive manufacturing”, *Composite Structures*, Elsevier Ltd, Vol. 176, pp. 547-555.
- Gay, D., Hoa, S.V. and Tsai, S.W. (2002), “Composite materials design and applications”, edited by CRC Press, available at: www.crcnetbase.com/isbn/9781420031683.
- Goglio, L., Rossetto, M. and Dragoni, E. (2008), “Design of adhesive joints based on peak elastic stresses”, *International Journal of Adhesion and Adhesives*, Vol. 28 No. 8, pp. 427-435.
- Goland, M. and Reissner, E. (1944), “The stresses in cemented joints”, *Journal of Applied Mechanics*, Vol. 11 No. 1, pp. A17-A27.
- IOSIPESCU and N (1967), “New accurate procedure for single shear testing of metals”, *J Mater*, Vol. 2, pp. 537-566.
- Kariz, M., Kuzman, M.K. and Sernek, M. (2017), “Adhesive bonding of 3D-printed ABS parts and wood”, *Journal of Adhesion Science and Technology*, Taylor & Francis, Vol. 31 No. 15, pp. 1683-1690.
- Koricho, E.G., Verna, E., Belingardi, G., Martorana, B. and Brunella, V. (2016), “Parametric study of hot-melt adhesive under accelerated ageing for automotive applications”, *International Journal of Adhesion and Adhesives*, Vol. 68, pp. 169-181.
- Liao, L., Huang, C. and Sawa, T. (2013), “Effect of adhesive thickness, adhesive type and scarf angle on the mechanical properties of scarf adhesive joints”, *International Journal of Solids and Structures*, Pergamon, Vol. 50 Nos 25/26, pp. 4333-4340.
- Loctite (2012), “TDS for new formulation of tratras® 401™”, available at: www.henkel.com/industrial (accessed 10 September 2021).
- Matweb (2021), “Overview of materials for cyanoacrylate adhesive”, available at: www.matweb.com/search/datasheettext.aspx?matguid=d0d7dbec7666421caf8aa08724b634c5 (accessed 13 December 2021).
- Mead, R., Gilmour, S.G. and Mead, A. (2012), “Statistical principles for the design of experiments: applications to real experiments”, available at: www.amazon.com/Statistical-Principles-Design-Experiments-Probabilistic/dp/0521862140 (accessed 3 November 2015).
- Montgomery, D.C. (2004), “Design and analysis of experiments”, *Design and Analysis of Experiments*, Wiley, John Wiley and Sons.
- Packham, D. (2003), “Surface energy, surface topography and adhesion”, *International Journal of Adhesion and Adhesives*, Vol. 23 No. 6, pp. 437-448.
- Roberson, D.A., Torrado Perez, A.R., Shemelya, C.M., Rivera, A., MacDonald, E. and Wicker, R.B. (2015), “Comparison of stress concentrator fabrication for 3D printed polymeric izod impact test specimens”, *Additive Manufacturing*, Elsevier, Vol. 7, pp. 1-11.
- Scarselli, G., Corcione, C., Nicassio, F. and Maffezzoli, A. (2017), “Adhesive joints with improved mechanical properties for aerospace applications”, *International Journal of Adhesion and Adhesives*, Elsevier, Vol. 75, pp. 174-180.
- Spaggiari, A. and Denti, F. (2019), “Mechanical strength of adhesively bonded joints using polymeric additive manufacturing”, *Proceedings of the Institution of Mechanical Engineers, Part C: Journal of Mechanical Engineering Science*, Vol. 235 No. 10, doi: [10.1177/0954406219850221](https://doi.org/10.1177/0954406219850221).
- Spaggiari, A., Castagnetti, D. and Dragoni, E. (2012), “Experimental tests on tubular bonded butt specimens: effect of relief grooves on tensile strength of the adhesive”, *The Journal of Adhesion*, Vol. 88 Nos 4/6, pp. 499-512. Taylor & Francis.
- Spaggiari, A., Castagnetti, D. and Dragoni, E. (2013), “Mixed-Mode strength of thin adhesive films: experimental characterization through a tubular specimen with reduced edge effect”, *The Journal of Adhesion*, Vol. 89 No. 8, pp. 660-675.
- Spaggiari, A., Castagnetti, D. and Dragoni, E. (2019), “A design oriented multiaxial stress-based criterion for the strength

- assessment of adhesive layers”, *Composites Part B: Engineering*, Vol. 157, doi: [10.1016/j.compositesb.2018.08.085](https://doi.org/10.1016/j.compositesb.2018.08.085).
- Spaggiari, A., Dragoni, E. and Brinson, H.F. (2016), “Measuring the shear strength of structural adhesives with bonded beams under antisymmetric bending”, *International Journal of Adhesion and Adhesives*, Elsevier, Vol. 67, pp. 112-120.
- Stojcevski, F., Hilditch, T. and Henderson, L.C. (2018), “A modern account of iosipescu testing”, *Composites Part A: Applied Science and Manufacturing*, Vol. 107 Elsevier Ltd, 1 April.
- Stratasys (2018), “Fortus 3D production systems”, available at: http://usglobalimages.stratasys.com/Main/Files/Machine_Spec_Sheets/PSS_FDM_FortusSystemsMaterialsOverview.pdf?v=635832637185031244 (accessed 6 December 2018).
- Stratasys (2019), “ABSplus-P430 mechanical properties”, available at: http://usglobalimages.stratasys.com/Main/Files/Material_Spec_Sheets/MSS_FDM_ABSplusP430.pdf (accessed 4 April 2019).
- Torrado Perez, A.R., Roberson, D.A. and Wicker, R.B. (2014), “Fracture surface analysis of 3D-printed tensile specimens of novel ABS-based materials”, *Journal of Failure Analysis and Prevention*, Springer, Vol. 14 No. 3, pp. 343-353.
- Tsai, M.Y. and Morton, J. (1995), “The effect of a spew fillet on adhesive stress distributions in laminated composite

- single-lap joints”, *Composite Structures*, Elsevier, Vol. 32 Nos 1/4, pp. 123-131.
- Ubaid, J., Wardle, B.L. and Kumar, S. (2018), “Strength and performance enhancement of multilayers by spatial tailoring of adherend compliance and morphology via multimaterial jetting additive manufacturing”, *Scientific Reports*, Vol. 8 No. 1, pp. 1-10.
- Vijaya Kumar, R.L., Bhat, M.R. and Murthy, C.R.L. (2013), “Evaluation of kissing bond in composite adhesive lap joints using digital image correlation: preliminary studies”, *International Journal of Adhesion and Adhesives*, Vol. 42, pp. 60-68.
- Wycherley, G.W., Mestan, S.A. and Grabovac, I. (1990), “Method for uniform shear stress-strain analysis of adhesives”, *Journal of Testing and Evaluation*, Vol. 18 No. 3, pp. 203-209.
- Zhang, Y., Sun, M.-J. and Zhang, D. (2012), “Designing functionally graded materials with superior load-bearing properties”, *Acta Biomaterialia*, Acta Materialia Inc., Vol. 8 No. 3, pp. 1101-1108.

Further reading

- Ng, C.T. and Susmel, L. (2022), “Notch static strength of additively manufactured acrylonitrile butadiene styrene (ABS)”, doi: [10.1016/j.addma.2020.101212](https://doi.org/10.1016/j.addma.2020.101212).

Appendix

This section reports the following Appendix. The CAD model and the picture of the test rig used to provide the correct alignment between the joints is shown in [Figure A1\(a\)](#) and [A1\(b\)](#), respectively. The charts with the stress strain curves

obtained on five specimens of the base material are reported in [Figure A2](#). The numerical data used in the ANOVA are showed in [Table A1](#) and the half normal plot on the peak force (N) and stiffness (N/mm) is presented in [Figure A3\(a\)](#) and [A3\(b\)](#), respectively. [Figure A3\(c\)](#) and [A3\(d\)](#) shows the interactions between the variable considered.

Figure A1 CAD model of the test rig used to enforce the specimen alignment (a) and experimental set-up (b)

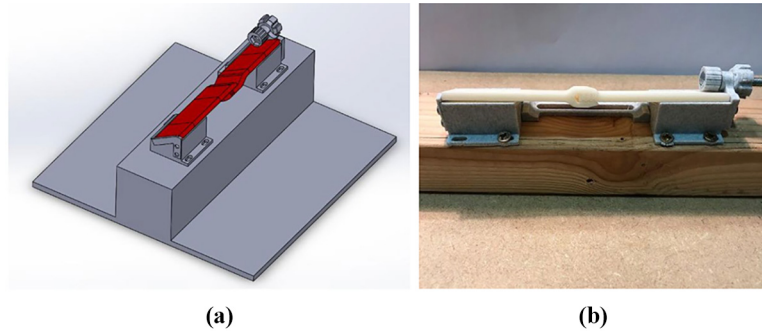


Figure A2 Stress-strain graph on dog-bone specimens made of base material and picture of the specimens after the tensile test

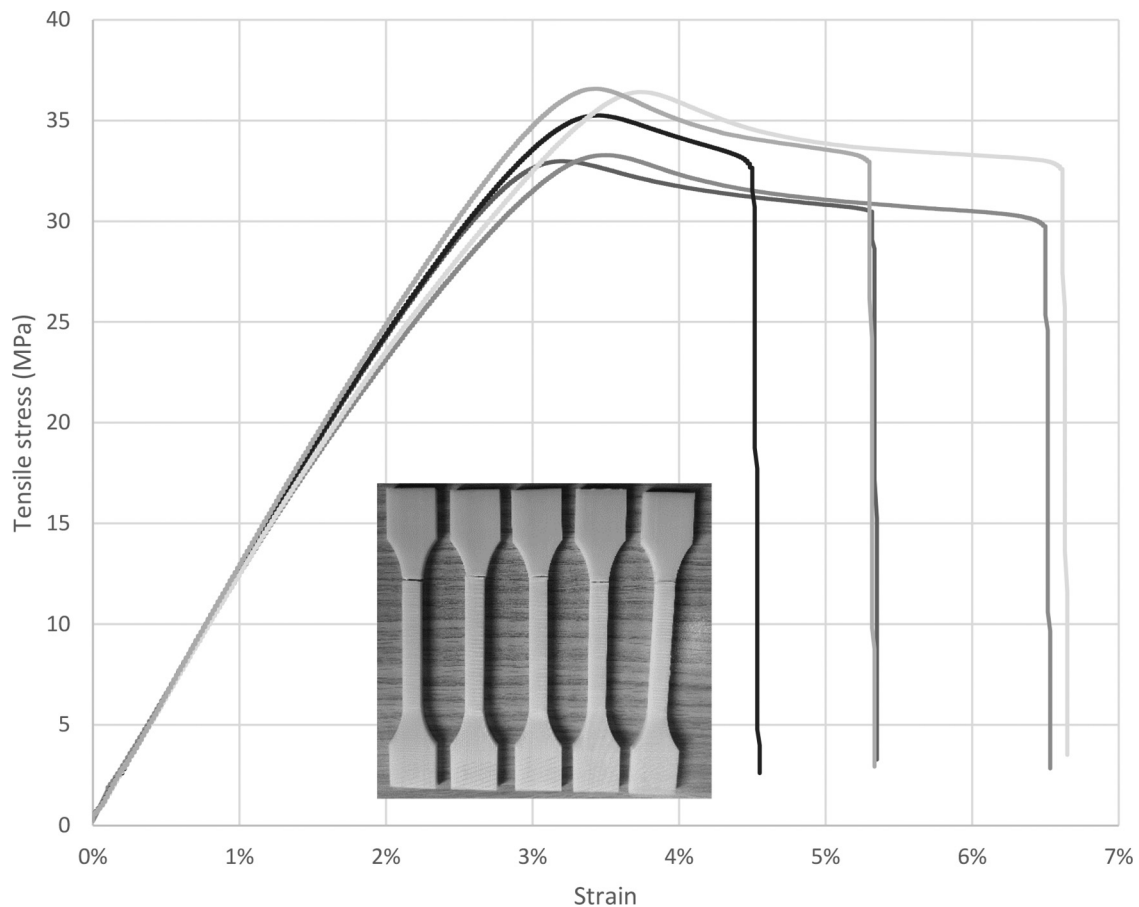
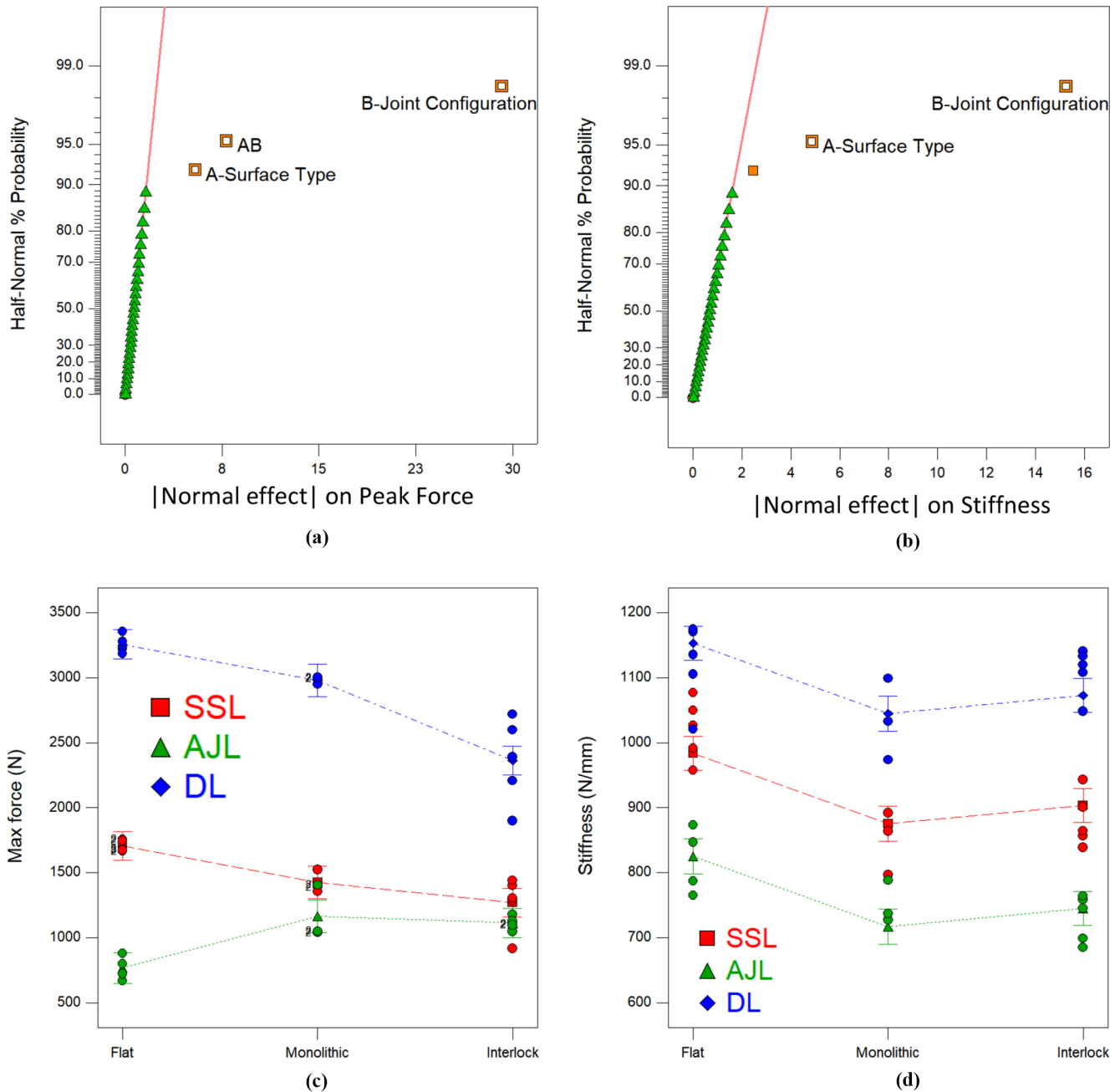


Table A1 Peak force and stiffness of the joints tested in the first experimental plan

Surface type	Peak force (N)	Stiffness (N/mm)
<i>Symmetric single lap</i>		
Flat	1747.53	1076.770833
Flat	1675.35	1049.75
Flat	1757.95	1026.604167
Flat	1666.22	991.9375
Flat	1685.13	957.8541667
Monolithic	1524.95	796.875
Monolithic	1357.1	863.9583333
Monolithic	1390.13	891.8333333
Interlocking	916.65	838.8541667
Interlocking	1307.05	943.3333333
Interlocking	1284.9	856.9791667
Interlocking	1441.22	901.2083333
Interlocking	1400.28	864.625
<i>Asymmetric joggle lap</i>		
Flat	670.4	873.2291667
Flat	880.23	846.9166667
Flat	722.53	787.5
Flat	799.6	765.2083333
Monolithic	1051.68	788.2291667
Monolithic	1040.2	737.1875
Monolithic	1407.65	727.7083333
Interlocking	1048.47	764.0208333
Interlocking	1131.43	745.3541667
Interlocking	1107.85	685.0625
Interlocking	1098.05	699.125
Interlocking	1180.63	758.5416667
<i>Double lap</i>		
Flat	3357.65	1170.85
Flat	3185.95	1174.78
Flat	3243.38	1105.45
Flat	3278.4	1020.75
Flat	3222.3	1135.65
Monolithic	2992.93	973.58
Monolithic	2950.03	1033.08
Monolithic	3002.98	1099.306931
Interlocking	1900.75	1140.564356
Interlocking	2207.15	1133.08
Interlocking	2600.53	1048.35
Interlocking	2718.48	1108.1
Interlocking	2391.43	1120.05

Figure A3 Normal effect of the variable on peak force (a) on Stiffness (b); interaction of the variables on the Peak Force (c) and on the Stiffness (d) for the three joints and surface type tested



Corresponding author

Andrea Spaggiari can be contacted at: andrea.spaggiari@unimore.it

For instructions on how to order reprints of this article, please visit our website:

www.emeraldgroupublishing.com/licensing/reprints.htm

Or contact us for further details: permissions@emeraldinsight.com